Dissociation Energies and Potential Energy Functions for the Ground $X\,^1\Sigma^+$ and 'Avoided-Crossing' $A\,^1\Sigma^+$ States of NaH

Sadru-Dean Walji, Katherine M. Sentjens and Robert J. Le Roy

Department of Chemistry,

University of Waterloo, Waterloo,

Ontario N2L 3G1, Canada;

(Dated: December 17, 2014)

A Direct-Potential-Fit analysis of all accessible data for the $A\,^1\Sigma^+ - X\,^1\Sigma^+$ system of NaH and NaD is used to determine analytic potential energy functions incorporating the correct theoretically predicted long-range behaviour. These potentials represent all of the data (on average) within the experimental uncertainties, and yield an improved estimate for the ground-state NaH well depth of $\mathfrak{D}_e = 15797.4\,(\pm 4.3)$ cm^{-1}, which is ~ 20 cm^{-1} smaller than the best previous estimate. The present analysis also yields the first empirical determination of centrifugal (non-adiabatic) and potential-energy (adiabatic) Born-Oppenheimer breakdown correction functions for this system, with the latter showing that the A-state electronic isotope shift is $-1.1\,(\pm 0.6)$ cm^{-1} going from NaH to NaD.

Suggested running head

Multi-isotopologue DPF analysis of NaH *or*
Full empirical analytic potentials for NaH

I. INTRODUCTION

Alkali hydrides are among the simplest diatomic molecules, and as such they are of great interest as testing grounds for theory. The one with the smallest reduced mass is LiH, for which 80 years of experimental studies[1–3] culminated the direct-potential fit (DFP) analysis by Coxon and Dickinson[4] which yielded quantum-mechanically accurate analytic potential energy function and Born-Oppenheimer breakdown (BOB) correction functions that explain all of the available data for all four isotopologues (on average) to within the experimental uncertainties. The next smallest alkali hydride is NaH, and determining analogous quantum-mechanically accurate potential energy and BOB correction functions for it was the objective of the present work.

While NaH has piqued interest as an observed molecule in exoplanet atmospheres in recent years,[5,6] it has been the object of study since the early 1930s.[7,8] As is illustrated by Fig. 1, the potential energy functions of the lower $^1\Sigma^+$ states of the alkali halides are governed by a series of avoided crossings as the outer walls of each of the lowest $^1\Sigma^+$ states in turn each takes on a substantial degree of ionic character.[2,9] In particular, the avoided crossing between the X- and A-state potentials gives rise to the unusual A-state well shapes that are more quartic than quadratic at the minimum, which gives rise to patterns of vibrational spacings and B_v values that initially increase with v. In addition, the analogous avoided crossings between the A and C states has the effect of causing the A-state potentials to be abruptly cut off in order to allow them to approach the $\mathrm{H}(1s) + alkali(np)$ asymptotes appropriately from below.

All previous empirical analyses of data for the $A\,^1\Sigma^+ - X\,^1\Sigma^+$ system of NaH were based on classical Dunham expansion fits,[10] sometimes followed by application of the first-order semiclassical Rydberg-Klein-Rees (RKR) inversion procedure[11,12] to obtain potential function points. In contrast, the present paper uses the fully quantum-mechanical 'direct-potential-fit' (DPF) procedure[13–15] to determine analytic potential energy functions for both the the $X\,^1\Sigma^+$ and $A\,^1\Sigma^+$ states that incorporate the correct theoretically known long-range behaviour,[16] together with centrifugal and potential energy BOB functions for both states.

II. OVERVIEW OF PREVIOUS WORK

NaH was first observed in 1930 by Hori who reported absorption bands of the $A\,^1\Sigma^+ - X\,^1\Sigma^+$ system spanning four vibrational levels of the X state and 18 levels of the A state,[7] In a paper on the NaH emission spectrum published the next year, he reported data for an additional band that he believed to be $0 \leftarrow 0$, increased all of his previous the A-state v' values by one unit,[8] and extended the range of the observed bands to span what was later shown to be[17] the range $v'(A) = 3 - 20$ for $v''(X) = 0 - 3$ The first NaD data were obtained by Olsson in 1934, and consisted of rovibrational

bands for $v''(X) = 0-1$ and $v'(A) = 7-17$, together with NaH measurements for $v''(X) = 0-1$ and $v'(A) = 7-17$. His first-order semiclassical analysis showed that Hori's revised v' numbering for NaH had to be increased by 3 units. Following Pesl *et al.*,[18] we have used uncertainties of ± 0.3 cm^{-1} to weight most of the 2430 observed NaH transitions of Hori[7,8] and Olsson[17], and ± 0.05 cm^{-1} for Olsson's 604 NaD transitions.[17]

After a decade of inactivity during World War II, work on this system resumed with Pankhurst's 1949 report of high temperature emission spectra of bands with $v''(X) = 3-8$ and $v'(A) = 1-7$ which had estimated line position uncertainties of ± 0.1 cm^{-1}, a factor of three smaller than that those for the earlier work.[7,8,17] Unfortunately, most of his data have been lost, and all we were left with is a Deslandres table of band origins, a list of A-state rotational constants, and tables of combination differences for $v''(X) = 3-8$ and $v'(A) = 1-7$ with $J = 1-32$. While the latter comprise remarkable sets of pseudo-microwave $S(J)$ data spanning a large range of J values for a wide range of $v''(X)$ and $v'(A)$ levels, they seem to have been overlooked in some later studies.[18]

After a further interregnum of 30 years, work on this system began in earnest in 1980 with Orth and Stwalley's observation of the $(v', v'') = (0,6) - (0,8)$ and $(1,6) - (1,8)$ bands in emission. Although their ± 0.1 cm^{-1} line position uncertainties were the same as those of Pankhurst,[19] they did provide the first direct observation of the lowest vibrational level of the $A\,^1\Sigma^+$ state. A year later, the first microwave data for this system was reported by Sastry *et al.*[20] While their data consisted of only the $R(0)$ line for each of $v''(\mathrm{NaH}) = 0-3$, the $R(1)$ and $R(2)$ lines for $v''(\mathrm{NaD}) = 0$ and the $R(2)$ line for $v''(\mathrm{NaD}) = 1-3$, its very high precision led to much improved low-order Dunham constants and the first examination of Born-Oppenheimer breakdown effects and deviations from first-order semiclassical reduced-mass scaling for this system. In 1987 this work was extended by Leopold *et al.*[21] who measured $R(J)$ transitions for $J = 0-6$ in $v = 0$,for $J = 0-7$ in $v = 1$, and for $J = 0-5$ in $v = 3$. Their work led to the determination of low-order molecular constants that were "... typically an order of magnitude more accurate than the best values previously available ...".[21]

The first infrared vibrational measurements for NaH were performed in 1988 by Magg and Jones using a tunable diode laser spectrometer.[22] The $\pm 0.001\,\mathrm{cm}^{-1}$ uncertainties of their data for 19 transitions of the vibrational fundamental and 7 transitions of the first hot band meant that when combined with the pure rotational data they yielded "... the most complete set of accurate values of the (low-order) ground-state Dunham parameters ..." to date.[22] A year later Maki and Olson[23] measured the infrared spectrum of NaH using a Fourier transform spectrometer and extended the data set to include transitions in the $3 \leftarrow 2$ band with uncertainties of $\pm 0.002\,\mathrm{cm}^{-1}$, This led to the determination of a further-improved set of Dunham constants and the first systematic determination of Born-Oppenheimer breakdown (BOB) parameters for this system. However, as

with all such parameter-expansion analyses, it was impossible to delineate between true BOB effects and and those due to breakdown of first-order semiclassical reduced-mass scaling.

Since 1990, all experimental studies of NaH or NaD have involved measurements of their ultraviolet $A\,^1\Sigma^+$-$X\,^1\Sigma^+$ spectra. First of all, in 1993 Rafi *et al.*[24] reported new measurements of $v''(X) = 0$ bands for $v'(A) = 13 - 22$, and of $v''(X) = 1$ bands for $v'(A) = 12 - 25$, in the form of band origins and A-state B_v and D_v rotational constants. Although their original line lists were lost,[25] since these measurements are the only observations of levels lying above $v'(A) = 20$, we chose to use their band origin data and to use their rotational constants to construct a set of synthetic pure rotational $\Delta J = 1 - 6$ A-state transitions for each of their bands, which we included in our data set. The uncertainties we associated with these synthetic data were ± 0.2 cm^{-1}, which is roughly the size of the uncertainties that Rafi *et al.*[24] had assigned to their their band origins. Three years later, Lochbrunner *et al.*[26] reported measurements of NaH band absorption from $v''(X) = 0-3$ into $v'(A) = 2 - 15$, and of NaD bands for $v''(X) = 0 - 2$ into $v'(A) = 5 - 17$. However, their results were only reported in the form of lists of band origins and $B_{v'}$ and $D_{v'}$ values and a new set of Dunham coefficients. Fortunately, the data for their $(v', 0) = (8, 0) - (15, 0)$ bands were obtained privately for inclusion in the later analysis of Pesl *et al.*,[18,27] but the data for their nine $v(A) > 0$ NaH bands and all of their twenty-five NaD bands are represented here only by their band origins. However, the precision of their results was only at the same *ca.* ± 0.3 level as the early data of Hori.[7,8] The first high resolution (± 0.006 cm^{-1}) electronic data for this system were those of Bahn et al. who reported the measurement of 141 transitions from $v(X) = 0$ and 1 into $v(A) = 3-9$ with $J'' = 0 - 30$.[28] Additional high-precision ($\pm 0.001 - 0.02$ cm^{-1}) UV data were later obtained by Pesl *et al.*[18] who applied a new variant of Doppler spectroscopy to laser-induced fluorescence from NaH molecules formed by reactive scattering of crossed beams of Na_2 and H atoms. They observed 280 transitions from bands for $v''(X) = 2 - 8$ and $v'(A) = 6 - 9$, and combined their results with all accessible earlier data to obtain a further improved sets of Dunham constants and RKR turning points.

Most recently, Huang *et al.*[29] used fluorescence depletion spectroscopy and stimulated emission pumping to delineate the properties of levels in the upper portion of the ground-state potential well. However, their analysis ignored the information about the $A\,^1\Sigma^+$ state that was contained in their data. In particular, they added the *differences* between their pump and probe laser frequencies to estimates of $X\,^1\Sigma^+$ state term values for the lower levels of their pump transitions that were calculated from the spectroscopic constants of Pesl *et al.*,[18] and fitted the resulting set of term values to conventional Dunham $(v+1/2)$ polynomials for G_v and B_v (ignoring centrifugal distortion). Their observation and inclusion of data for $v(X) = 21$ certainly made their X-state analysis the most comprehensive to date. However their neglect of the older data and of the information about

the $A\,^1\Sigma^+$ state, and their reliance on term values generated from previously reported molecular constants[18] rather than on the actual data on which they were based, were weaknesses of their approach.

In all previous studies of this system, the analyses were based on the historic Dunham model,[10,30] and with two exceptions,[20,23] when isotope effect were considered at all it was assumed that they could be accounted for by first-order semiclassical reduced-mass scaling.[10,13] In contrast, the present work reports the first DPF analysis of this system. In contrast with the traditional parameter-fitting Dunham-type treatments, the DPF method is fully quantum-mechanical, and its results consist of analytic expressions for the potential energy curves and any relevant BOB functions for the state(s) in question. BOB effects are particularly important in molecules with small reduced mass, especially hydrides, and a combined-isotopologue DPF analysis allows them to be taken into account properly. In addition, the $A\,^1\Sigma^+$ of the alkali hydrides is known to have an abnormal 'truncated' potential energy curve, and for such cases no finite Dunham expansions can readily represent all of its level energies, while a DPF analysis using an appropriate model potential form can. The purpose of this paper is therefore to present a combined-isotopologue DPF analysis of all available data for this system that yields highly accurate and compact analytic representations of the potential energy curves for the $X\,^1\Sigma^+$ and $A\,^1\Sigma^+$ of NaH.

III. SELECTION AND TREATMENT OF DATA

The properties and sources of the data used in the present analysis are summarized in Table 1. The uncertainties shown there were in general taken from the appropriate experimental paper and were used for all lines from that source, with the following exceptions. In the case of the electronic band data, if a line had a discrepancy much larger than its neighbours and another line in that data set had the same energy, its uncertainty was multiplied by a factor of three. Similarly, if a relatively large discrepancy was encountered, and the line was associated with the highest observed J-level in that branch, it's uncertainty was multiplied by a factor of two. These two modifications affected, respectively, 58 and 3 lines of the 1906 Hori hydride data,[7,8] while the first affected 11 line of the 604 Olsson NaD data.[17] Finally, if a line had a discrepancy from our best-fit model of more that 8 times the average uncertainty for its band/group, we concluded that it was an outlier (possibly mis-assigned), and de-weighted it out of the final fits. This led to removal of 1 Hori NaH datum, 13 Olsson NaD data, 5 Pesl *et al.* NaH data, 4 of the Pankhurst 'combination difference' pure rotational data, and 15 of the Bahn *et al.* data, including the three assigned to $v' = 10$ and 12 for which the discrepancies of > 10 cm^{-1} show that they were completely mis-identified. Moreover, while all of the synthetic $A\,^1\Sigma^+$-state pure rotational Rafi[24] data were consistent with our best models (within the assumed 0.2 cm^{-1} uncertainties), the discrepancies for his band origins for $v(A) = 0 - 20$ led

us to assign them uncertainties of ± 1 cm^{-1}, while the much larger discrepancies (increasing from -4 to -60 cm^{-1}) for his 7 $v(A) = 21 - 25$ band origins led us to deweight them completely out of the final data set. All of the other older (pre 2010) data retained in our analysis were weighted by the uncertainties shown in column-3 of Table 1, while numbers of data shown in its column-7 are the numbers used in the final analysis.

The present work utilizes the data of Huang *et al.*[29] in a much more direct way than they did.[31] First of all, following their approach we use the *differences* between their pump and probe transition energies to define a set of 286 pseudo vib-rotation transitions from levels with $v(X) = 0$ and $J = 0 - 14$ into those with $v(X) = 9 - 21$. However, rather than represent the properties of the lower levels of the X state by a previously reported set of Dunham expansion parameters, we have relied in our inclusion of all of the earlier data for this system to define the lower portion of that potential energy well. Moreover, rather than neglect information about the A state, we have also included their 50 'pump' transitions from $v(X) = 0$ and 9 into $v(A) = 7 - 12$ and their 277 $v(A) = 7 - 12$ into $v(X) = 9 - 21$ 'probe' transitions as separate data. As shown in Table 1, we have assigned uncertainties of 1.0, 3.0, and 2.0 cm^{-1} to these three components of their data, within which they are in good agreement with our best models. Listings of our entire data set and of the differences between those data and our recommended model are included in the Supplementary Material associated with this paper.[32]

IV. DIRECT-POTENTIAL-FIT DATA ANALYSIS

A. The Radial Hamiltonian

Most spectroscopic data may be described in terms of differences between eigenvalues of potential energy function(s) for the electronic state(s) involved in the transition. However, for species of small reduced mass, especially hydrides, Born-Oppenheimer breakdown (BOB) effects give rise to differences between the effective potential energy functions for different isotopologues, and introduce isotopologue-dependent corrections to the 'mechanical' centrifugal potential. The present work uses Watson's formulation of this problem,[33,34] in which the effective radial Schrödinger equation for isotopologue-α of a diatomic molecule A-B may be written the form:[35]

$$\begin{aligned} \widehat{\mathcal{H}}\ \psi_{v,J}(r) \ = \ & \left\{ -\frac{\hbar^2}{2\mu_\alpha}\frac{\mathrm{d}^2}{\mathrm{d}r^2} \ + \ \left[V_{\mathrm{ad}}^{(1)}(r) + \Delta V_{\mathrm{ad}}^{(\alpha)}(r) \right] \right. \\ & \left. + \ \frac{[J(J+1)]\hbar^2}{2\mu_\alpha r^2}\left[1 + g^{(\alpha)}(r)\right] \right\} \psi_{v,J}(r) \ = \ E_{v,J}\ \psi_{v,J}(r) \ . \end{aligned} \tag{1}$$

Here, $V_{\mathrm{ad}}^{(1)}(r)$ is the effective adiabatic internuclear potential for a chosen reference isotopologue (denoted $\alpha = 1$), $\Delta V_{\mathrm{ad}}^{(\alpha)}(r)$ is the difference between the effective adiabatic potential for isotopologue-α and that for the chosen reference isotopologue, μ_α is the normal reduced mass of atoms A and B

with masses $M_A^{(\alpha)}$ and $M_B^{(\alpha)}$, and $g^{(\alpha)}(r)$ is the effective non-adiabatic correction term to the centrifugal potential for isotopologue α. As was shown by Watson $\Delta V_{\rm ad}^{(1)}(r)$ and $g^{(\alpha)}(r)$ may each be written a sum of terms associated with the two atoms.[33,34] We find it most convenient to express those terms using the mass-difference and mass-ratio representation of Ref. 35:

$$\Delta V_{\rm ad}^{(\alpha)}(r) \;=\; \frac{\Delta M_{\rm A}^{(\alpha)}}{M_{\rm A}^{(\alpha)}}\;\widetilde{S}_{\rm ad}^{\rm A}(r) \;+\; \frac{\Delta M_{\rm B}^{(\alpha)}}{M_{\rm B}^{(\alpha)}}\;\widetilde{S}_{\rm ad}^{\rm B}(r) \quad . \tag{2}$$

$$g^{(\alpha)}(r) \;=\; \frac{M_{\rm A}^{(1)}}{M_{\rm A}^{(\alpha)}}\;\widetilde{R}_{\rm na}^{\rm A}(r) \;+\; \frac{M_{\rm B}^{(1)}}{M_{\rm B}^{(\alpha)}}\;\widetilde{R}_{\rm na}^{\rm B}(r) \quad , \tag{3}$$

in which $\Delta M_{\rm A/B}^{(\alpha)} \;\equiv\; M_{\rm A/B}^{(\alpha)} - M_{\rm A/B}^{(1)}$ is the difference between the masses of atom A or B in isotopologue-α and in the reference isotopologue, $\widetilde{S}_{\rm ad}^{\rm A/B}(r)$ represents the 'adiabatic' potential-energy BOB correction function for atom A or B, and $\widetilde{R}_{\rm ad}^{\rm A/B}(r)$ is the 'non-adiabatic' centrifugal BOB radial strength function for atom A or B.

B. Data Analysis Procedure

The present analysis involved application of a standard DPF procedure.[14,15,36] Observed transition energies are compared to eigenvalue differences generated by solving Eq. (1) using parameterized analytic trial potential energy and BOB functions, and a standard non-linear least-squares procedure is used to optimize those parameters.[14] The partial derivatives of the eigenvalues with respect to the parameters of the model required by this procedure are readily calculated using the standard Hellmann-Feynman theorem expression: $\frac{\partial E_{v,J}}{\partial p_j} = \left\langle \psi_{v,J}(r) \left| \frac{\partial V(r)}{\partial p_j} \right| \psi_{v,J}(r) \right\rangle$. The initial trial potential-function parameters required to initiate such fits may be generated by fitting the chosen functional form form to a set of turning points generated by application of the familiar semiclassical 'RKR' inversion procedure[11,12] to a conventional set of molecular constants, or by *ab initio* calculations.[37]

For a given model, we characterize the quality of fit by the 'dimensionless root-mean-square deviation', which we define by the expression

$$\overline{dd} = \sqrt{\frac{1}{N}\sum_{i=1}^{N}\left(\frac{y_i^{calc} - y_i^{obs}}{u_i}\right)^2}. \tag{4}$$

in which N is the total number of data, $y_i^{\rm calc}$ is the the value of datum i calculated from the given trial model and the corresponding experimental quantity $y_i^{\rm obs}$, and u_i is the estimated uncertainty in the experimental value for datum-i. A 'good' fit is a case for which $\overline{dd} \lesssim 1$. However, if $\overline{dd}$ is persistently significantly greater than unity for a particular subset of the data, independent of the number of free parameters in the model, it usually means that the estimated uncertainties for that

group of data are too small, and should be increased. This was the basis of the data-weighting/data-selection procedure described in Section III.

C. The Potential Energy Function Form

It is well known that the outer walls of the potential energy wells of the $A\,^1\Sigma^+$ states of all of the alkali hydrides change shape abruptly, just before they rise past the energy of the alkali $nP_{1/2}$ atomic state, because of an avoided crossing between a strongly attractive $^1\Sigma^+$ 'diabatic' ion-pair state and a $^1\Sigma^+$ van der Waals state that dissociates to the alkali $nP_{1/2} + \mathrm{H}(^2S)$ threshold (see Fig. 1).[2,9,38] Because this unusual behaviour would seem to preclude normal merging to inverse-power-sum long-range behaviour, we have chosen to represent the potential energy function for this state by an 'Expanded Morse Oscillator' (EMO) function. This function has the form of a simple Morse potential in which the exponent coefficient is a function of distance:

$$V_{\mathrm{EMO}}(r) = \mathfrak{D}_e \left(1 \; - \; e^{-\beta_{\mathrm{EMO}}(r)\cdot(r-r_e)}\right)^2 \quad , \tag{5}$$

in which $\mathfrak{D}_e$ is the well depth, r_e is the equilibrium internuclear distance, and the exponent coefficient

$$\beta_{\mathrm{EMO}}(r) \; = \; \sum_{i=0}^{N_\beta} \beta_i \, y_q^{\mathrm{ref}}(r)^i \tag{6}$$

is a power series in a dimensionless variable:

$$y_q^{\mathrm{ref}}(r) \; = \; \frac{r^q - r_{\mathrm{ref}}^q}{r^q + r_{\mathrm{ref}}^q} \tag{7}$$

that is defined by a selected expansion centre r_{ref} and power q.

The free fitting parameters of this potential form are $\mathfrak{D}_e$, r_e, and the expansion coefficients β_i of Eq. (6), while the values of N_β, q, and r_{ref} are optimized manually. There are no rules governing the choice of q and r_{ref} other than that experience shows that 'too small' values of the former ($q \lesssim 2$) sometimes lead to potential functions that behave badly in the extrapolation region(s) outside the 'data range', the region bounded by the inner and outer turning points of the highest vibrational level involved in the analysis, and that we would normally expect the latter to lie within the this 'data range'. The geometric mean of those two turning points is usually a good initial trial value for r_{ref}.

In contrast with the $A\,^1\Sigma^+$ state, the potential energy function for the $X\,^1\Sigma^+$ state of NaH *is* expected to show the normal merging to inverse-power-sum long-range behaviour, so we represent it by the Morse/Long-Range (MLR) function that has the general form of a Morse-type potential with two key differences: (i) the exponent distance factor $(r - r_e)$ is replaced by a dimensionless variable that is also linear in r near r_e but approaches a constant as $r \to \infty$, and (ii) and there

is a pre-factor in front the exponential term that defines the long- and very-short-range behaviour of the potential. This function has the form:

$$V_{\rm MLR}(r) = \mathfrak{D}_e \left(1 \; - \; \frac{u_{\rm LR}(r)}{u_{\rm LR}(r_e)} \; e^{-\beta_{\rm MLR}(r) \cdot y_p^{\rm eq}(r)} \right)^2 \quad , \tag{8}$$

in which $\mathfrak{D}_e$ and r_e are as defined above, while the radial distance variable has the same form as that of Eq. (7), except that it is defined by an expansion centre of r_e and a different integer power, p:

$$y_p^{\rm eq}(r) = \frac{r^p - {r_e}^p}{r^p + {r_e}^p} \quad . \tag{9}$$

The exponent coefficient function in Eq. (8) is then defined by the expression:

$$\beta_{\rm MLR}(r) \; = \; \beta_{p,q}^{\rm ref}(r) \; = \; y_p^{\rm ref}(r) \, \beta_\infty \; + \; \left[1 - y_p^{\rm ref}(r) \right] \; \sum_{i=0}^{N_\beta} \beta_i \, y_q^{\rm ref}(r)^i \quad , \tag{10}$$

in which

$$\beta_\infty \; \equiv \; \ln \left\{ \frac{2 \, \mathfrak{D}_e}{u_{\rm LR}(r_e)} \right\} \; = \; \lim_{r \to \infty} \beta(r) \quad , \tag{11}$$

and the expansion variable $y_q^{\rm ref}(r)$ is again defined by Eq. (7) while the variable $y_p^{\rm ref}(r)$ has that same form, but is defined by the same power p used to characterize the radial distance variable of Eq. (9), rather than by q (although one could choose to set $q = p$). The three dimensionless radial variables are defined as they are because of the effect of the integer powers p and q on the long-range behaviour of the exponential term in Eq (8).[39]

A key property of the form of Eqs. (8–11) is the fact that the above definition of β_∞ means that the long-range behaviour of an MLR potential is:

$$V_{\rm MLR} \; \simeq \; \mathfrak{D}_e - u_{\rm LR}(r) + \mathcal{O}\{u_{\rm LR}(r)^2/(4\mathfrak{D}_e)\} \quad . \tag{12}$$

The pre-factor to the exponential term in Eq.(8) is generally defined by the expression:

$$u_{\rm LR}(r) \; = \; \sum_{m=m_1}^{m_{\rm last}} \; D_m(r) \; \frac{C_m}{r^m} \tag{13}$$

in which $\{m\}$ are the powers of the leading inverse-power terms that theory dictates define the limiting long-range behaviour of the particular molecular state, and the associated coefficients C_m are (usually) known from theory. The associated 'damping functions' $D_m(r)$ were introduced to model the weakening of long-range dispersion energies due to electron overlap at shorter distances.[39,40] Following Ref. (39), we have chosen to represent them by the generalized Douketis-type[41] functions

$$D_m(r) \; = \; \left[1 \; - \; \exp\left(-\frac{b(\rho r)}{m} - \frac{c(\rho r)^2}{m^{1/2}} \right) \right]^{m-1} \quad , \tag{14}$$

in which $b = 3.30$ and $c = 0.423$,[39] and which have the convenient complementary property that

$$\lim_{r\to 0}\{\, D_m(r)/\, r^m\}\ \ \propto\ r^{-1}\ \ , \tag{15}$$

which in turn means that the limiting short-range behaviour of the repulsive wall of our potential will be $\propto 1/r^2$.[39] The constant ρ in Eq. (14) is a system-dependent parameter used to account for the sizes of the electron clouds on the interacting atoms. Following Ref. 41, for interacting atoms A and B:

$$\rho \equiv \rho_{\rm AB}\ =\ \frac{2\rho_{\rm A}\rho_{\rm B}}{(\rho_{\rm A}\ +\ \rho_{\rm B})} \tag{16}$$

in which $\rho_{\rm A} = (I_p^{\rm A}/I_p^{\rm H})^{2/3}$ is defined by the ratio of the ionization potential $I_p^{\rm A}$ of atom A to that of a ground-state H atom, $I_p^{\rm H}$. For the case of ground-state H and Na atoms, $\rho = \rho_{\rm NaH} = 0.69$, the leading terms in Eq. (13) correspond to $m = 6$, 8, and 10, and we are fortunate to have the excellent values for those C_m coefficients reported by Mitroy and Bromley[16] to define the long-range tail function $u_{\rm LR}(r)$ of our MLR potential for ground-state NaH.

The free fitting parameters in the MLR model are $\mathfrak{D}_e$, r_e and the β_i expansion parameters of Eq. (10), while the values of N_β, p, q and $r_{\rm ref}$ are set manually and the C_m values are fix at their theoretical values.[16] The only firm constraint on the values of the integer powers p and q is that the power p must be larger than the difference between the last and first powers in the (damped or undamped) inverse-power sum of Eq. (13), $p > (m_{\rm last} - m_i)$, in order to prevent the long-range behaviour of the exponential term in Eq. (8) from affecting that defined by the expansion of Eq. (13). However, as with the EMO potential form, 'small' values of q ($q \lesssim 2$) sometimes tend lead to potential functions that behave badly in the extrapolation region(s) outside the 'data range', while too-large values make the $y_q^{\rm ref}(r)$ expansion variable somewhat 'stiff', so that larger values of the power N_β are required to give an equivalently 'good' potential energy function.

D. BOB Radial Strength Function Forms

Following Ref. 42, the radial strength functions characterizing the atom-dependent potential-energy and centrifugal BOB corrections of Eqs. (2) and (3) are expanded in the same form utilized for the exponent coefficient-function of the MLR potential:

$$\widetilde{S}_{\rm ad}^{\rm A}(r)\ =\ y_{p_{\rm ad}}^{\rm eq}(r)\ u_\infty^{\rm A}\ +\ [1-y_{p_{\rm ad}}^{\rm eq}(r)]\ \sum_{i=0}^{N_{\rm ad}^{\rm A}} u_i^{\rm A}\ y_{q_{\rm ad}}^{\rm eq}(r)^i\ \ , \tag{17}$$

$$\widetilde{R}_{\rm na}^{\rm A}(r)\ =\ y_{p_{\rm na}}^{\rm eq}(r)\ t_\infty^{\rm A}\ +\ [1-y_{p_{\rm na}}^{\rm eq}(r)]\ \sum_{i=0}^{N_{\rm na}^{\rm A}} t_i^{\rm A}\ y_{q_{\rm na}}^{\rm eq}(r)^i\ \ . \tag{18}$$

Since NaH is not an ion, $t_\infty^A = t_\infty^B = 0$ for both the $X\,^1\Sigma^+$ and $A\,^1\Sigma^+$ states.[42] Moreover, since we adopt the convention of defining the absolute zero of energy as the energy of ground state atoms

at infinite separation, by definition, $u_\infty^A = u_\infty^B = 0$ for all molecular states that dissociate to that limit, and since Na has only one stable isotope, this is also true for the $A\,^1\Sigma^+$ state.[42] Within this convention, the values of $u_0^{\rm A/B}(X)$ define the isotopologue-dependence of the ground state well depth. However, since Na has only one isotope, necessarily $u_0^{\rm Na}(X) = 0$, and since the NaD data for the $X\,^1\Sigma^+$ state span only a small fraction ($\lesssim 23\%$) of the well we cannot expect to be able to determine the H/D isotope dependence of that well depth from these data, so we also fixed $u_0^{\rm H}(X) = 0$. However, our fitted value of $u_0^{\rm H}(A)$ (see below) provides the best current estimate of the H/D electronic isotope shift for the $A - X$ system.

Other than the general caveat (see above) that too small values may lead to unphysical behaviour in the extrapolation regions outside the 'data range', while too large values may tend to a need for higher polynomial orders in Eqs. (17) and (18), there are no explicit constraints on the values of $p_{\rm na}$, $q_{\rm na}$, $q_{\rm ad}$, However, since $p_{\rm ad}$ defines the limiting inverse-power long-range behaviour of the $\widetilde{S}_{\rm ad}^{\rm A}(r)$ functions, it should be set equal to the power of the leading term in Eq. (13), $p_{\rm ad} = m_1$ to ensure that the effective adiabatic potentials $V_{\rm ad}^{(\alpha)}$ have the same limiting long-range functional behaviour for all isotopologues.

V. RESULTS

A. Preliminary $X\,^1\Sigma^+$ Single-State Analysis

Because of the unusual shape of the $A\,^1\Sigma^+$-state potential function, we began our analysis with fits that treated all of its vibration-rotation levels as independent term values. This allowed us to optimize our representation of the potential energy and centrifugal BOB functions for the $X\,^1\Sigma^+$ state, independent of any assumptions about a representation for the $A\,^1\Sigma^+$ state. Moreover, since the highest observed levels of the $A\,^1\Sigma^+$ state lie more than 1000 cm^{-1} below its asymptote, and the distance between the potential asymptotes is the accurately known atomic excitation energy of Na, this will have no significant effect on the determination of the ground-state dissociation energy.

The lower panel of Fig. 2 shows how our quality-of-fit parameter $\overline{dd}$ varies with the order of the MLR exponent polynomial $N = N_\beta$ and the location of expansion the centre $r_{\rm ref}$ for four different combinations of the expansion coefficient powers p and q. As expected, we see that for *any* choice of $r_{\rm ref}$ increasing N_β improves the quality-of-fit, and that all four families of models seem to be converging to the same optimum value of $\overline{dd}$. Following the arguments presented at the end of Section IV.C, the cases considered in Fig. 2 all involve $p > (m_{\rm last} - m_1) = 4$, and the values of q are all > 2. However, there are no obvious trends with p or q.

In addition to minimizing $\overline{dd}$ for the smallest possible number of parameters, a key criterion in selecting an optimum potential function model is that it should behave sensibly in the extrapolation interval past the outer end of the data region. A simple way of testing for that is to examine the

behaviour of a plot of $\left\{C_6^{\rm eff}(r) \equiv r^6[\mathfrak{D} - V_{\rm MLR}(r)]\right\}$ vs. $1/r^2$. The structure of Eqs. (12) and (13) means that as $1/r^2 \to 0$ ($r \to \infty$), plots of this type must approach an intercept of $C_6^{\rm theory}$ with a slope of $C_8^{\rm theory}$, where $C_m^{\rm theory}$ are the values of the fixed coefficients defining the two leading terms in the expansion of Eq. (13). Figure 3 shows that all of the potentials considered there do have this expected limiting behaviour, but that the models for which $p = 5$ tend to dip down and approach the limiting slope from below. This is unphysical, since the leading deviation from the limiting (linear) behaviour should show positive curvature, due to the positive (attractive) $C_{10}^{\rm theory}$ term in the long-range potential. We therefore select an MLR function with $N = N_\beta = 12$, $p = 6$, $q = 4$ and $r_{\rm ref} = 3.0$ (circled points on Fig. 2) as our recommended model for the potential energy function of the $X\,^1\Sigma^+$ state of NaH.

The Upper Panel of Fig. 2 shows that the model-dependence of the fitted values of the ground-state well depth $\mathfrak{D}_e$ is far larger than the uncertainties in virtually any of the values yielded by the individual fits. In order to obtain a the best possible estimate of the overall uncertainties in the physically interesting parameters $\mathfrak{D}_e$ and r_e, we therefore adopted the averaging-over-models procedure of Eqs. (6)–(8) of Ref. 43 (or Eqs. (21-23) of Ref. 15). On averaging over the results for the 63 cases the for which the value of $\overline{dd}$ was no more that 1% larger than that for the recommended model (points below the $+1\%$ line in the lower panel of Fig. 2), we obtain $unc\{\mathfrak{D}_e\} = 4.3\,{\rm cm}^{-1}$ and $unc\{r_e\} = 0.0000015\,$Å. Extending this averaging to include result for the 82 models whose $\overline{dd}$ values were within 2% of that for the recommended model (points below the $+2\%$ line in the lower panel of Fig. 2) lowers the $\mathfrak{D}_e$ uncertainty in its second decimal place and raises that in r_e to $0.0000020\,$Å. The shaded region in the upper panel of Fig. 2 indicates the band of uncertainty associated with averaging over the 63 models associated with the 1% limit.

With an optimum X-state potential function model selected based on the fits to NaH data alone described above, we undertook a preliminary attempt to determine the number of BOB terms required to simultaneously explain those data. This study showed that either three or four potential-energy BOB terms and one centrifugal BOB term would be required. However, because of the expected high degree of correlation between the numbers and values of the BOB parameters for the X and A states, the delineation of optimum BOB models for the $X\,^1\Sigma^+$ state had to await the global two-state analysis described below.

B. Two-State Analysis and Determining the $A\,^1\Sigma^+$ State Potential Energy Function

Using the recommended model for the $X\,^1\Sigma^+$-state potential determined above, we then proceeded to perform full two-state, 2-isotopologue fits to determine an optimum model for the $A\,^1\Sigma^+$ potential energy function. As discussed at the beginning of section IV.C, we have chosen to use an

EMO function to represent the potential function for this state. While the values of $\mathfrak{D}_e$, r_e and the well-shape parameters β_i are all determined automatically using our least-squares fitting program DPotFit,[14] as with the $X\,^1\Sigma^+$-state fits described above, optimum values for the expansion centre $r_{\rm ref}$ and power q defining the dimensionless radial variable of Eq. (7) were determined manually. One general finding was that for $q = 2$ or 3, all of the fitted EMO potentials had an inflection point on the inner wall above the potential asymptote, which led to a spurious inner maximum and potential function turnover in the short-range extrapolation region, so those models were physically unacceptable. This was also true for the $q = 4$, $N_\beta = 17$ models for $r_{\rm ref} < 2.9\,$Å. However, the remaining $N_\beta = 17$, $q = 4$ models, all of the $q = 4$, $N_\beta = 15$ and 16 models, and all of the $q = 5$ models considered, had physically sensible short-range walls with strictly positive curvature.

Figure 4 show how the quality-of-fit parameter $\overline{dd}$ for the global fit varies with the EMO exponent polynomial order $N = N_\beta$ and with the expansion variable parameters q and $r_{\rm ref}$. As is seen there, the $q = 5$ models (solid points joined by dashed lines) require more β_i expansion parameters to achieve a given quality of fit than do those for $q = 4$ (open filled points joined by solid lines), and do not even approach the $q = 4$ results for the range of $N = N_\beta$ values considered. Because of the close convergence of the $N_\beta = 16$ and 17 models at their common $\overline{dd}$ minima, we choose the $N_\beta = 16$, $q = 4$ EMO function for $r_{\rm ref} = 3.0\,$Å as our recommended potential energy function for the $X\,^1\Sigma^+$ state of NaH. Figure 4 is a much simpler picture than Fig. 2 because the EMO potential has only one integer expansion-variable parameter to vary, while the MLR form has two, and we chose to omit plots for small values of N_β. Moreover, since the distance between their potential asymptotes is determined by the accurately known Na($3s \rightarrow 3p$) atomic excitation energy,[44] the value of and uncertainty in the $A\,^1\Sigma^+$ well depth are determined by those for the $X\,^1\Sigma^+$ state, so the analog of the upper panel of Fig. 2 would carry little new information.

The final stage of the analysis consisted of our optimizing the forms of the expansion variables and numbers of expansion parameters defining the BOB functions for the two states. This is a relatively straightforward procedure, since the fact that their effects are quite small relative to those of the potential function parameters means that at worst, only order-of-magnitude trial parameters are requires to initiate stable, unique least-squares fits (indeed, trial parameter values of 0.0 usually suffice!). Note, however, that the limited vibrational range of the deuteride data does not allow a physically significant determination of the well depths for the deuterium isotopologues, so the values of $u_0^{\rm H}$ for the two states are 100% correlated. In particular, either one (or their difference) could serve to define the single experimental observable, the electronic isotope shift. In the analysis reported here we chose arbitrarily to fix $u_0^{\rm H}(X) = 0.0$, which means that all of this isotope shift is attributed to the isotopologue-dependence of the A-state well depth. However, this ansatz could readily be changed if additional data were obtained that would allow a reliable independent determination of

one of the deuteride well depths. Since the centrifugal BOB corrections for the two states both affect high-J electronic data in similar ways, one might expect these functions to also be fairly highly correlated. However, a trial-and-error procedure quickly led to an optimum model here too.

The parameters defining our recommended analytic potential energy functions for the $X\,^1\Sigma^+$ and $A\,^1\Sigma^+$ states of NaH are presented in Table II. Numbers in parentheses are 95% confidence limit uncertainties in the last digits shown, obtained by application of the averaging-over-models procedure described above to models whose $\overline{dd}$ values lie within 1% of the minimum value. After application of the 'sequential rounding and refitting' (SRR) scheme of Ref. 46 minimized the numbers of digits required to define the model with no signigicant loss of accuracy ($< 0.04\%$ increase in $\overline{dd}$), the final fit to 5263 data, and yielded $\overline{dd} = 1.21591$. A Fortran subroutine for generating the effective potential energy and centrifugal potential functions for either isotopologue in either state is included with the Supplementary Material accompanying this manuscript.[32] This supplementary material also includes listings of the eight leading "band constants" (the vibrational energies and first 7 rotational constants) for all vibrational levels of both isotopologues supported by these two potentials, together with sample input data files for the standard vibrational-eigenvalue/Franck-Condon 'LEVEL'.[45]

The lower panel of Fig. 5 compares our spectroscopically-accurate empirical potential energy functions for the $X\,^1\Sigma^+$ and $A\,^1\Sigma^+$ states of NaH with the *ab initio* potentials of Aymar, Deiglmayr and Dulieu[9] (points). On the scale of this figure the degree of agreement is remarkably good, although the minimum and inner wall of the *ab initio* potential for the A-state state appear to lie at slightly smaller distances than are dictated by the experimental data. The upper panel of Fig. 5 then shows the 95% confidence limit uncertainty in the final potentials, as calculated from the parameter uncertainties and correlation matrix of the fit using standard expressions (see, e.g., Eq. [7] of ref.46). As may be expected, the uncertainty in the A-state potential goes through a maximum in the extrapolation region between the outer turning point of the highest observed level and the asymptote. This does not occur for the ground state, as the outer end of its data region lies at relatively large r where the overall interaction energy is going to zero. As may be expected, the uncertainties in both potentials become quite large beyond the inner ends of their respective data regions which lack the limiting constraint of having to approach an asymptote.

VI. CONCLUSION AND DISCUSSION

A global DPF analysis of all available data for the $A\,^1\Sigma^+ - X\,^1\Sigma^+$ systems of NaH and NaD has yielded accurate analytical potential energy functions and Born-Oppenheimer breakdown functions for these two states that (on average) reproduce all of the data within the experimental uncertainties. Figure 5 shows that these potential functions are in excellent agreement with the best available *ab*

initio calculations for these states. It is particularly gratifying to see the close agreement of our fitted A-state EMO function with the *ab initio* points in the extrapolation region past the outer turning point for $v_A = 25$, which marks the outer end of the A-state data region, as this demonstrates the ability of this functional form to accommodate the abrupt change of potential function character associated with the avoided crossing that takes this state to the Na($3p$)+H($1s$) limit (see Fig. 1) and gives rise to the abrupt cut-off of the $\Delta G_{v+1/2}$ plot seen in Fig. 6.

Our analysis confirms that $v = 21$ (bound by 18.9 cm^{-1}) is indeed the last bound level of the ground state of NaH, and predicts that $v = 29$ (bound by 34.6 cm^{-1}) is the highest vibrational level of ground-state NaD. While the uncertainty in $\mathfrak{D}_e$ may make the significance of these estimates somewhat uncertain, the scattering lengths implied by our potentials for ground-state NaH and NaD are 0.392 and x.xx Å, respectively. Similarly, our analysis predicts that the highest vibrational levels of the $A\,^1\Sigma^+$ states of NaH and NaD are $v = 32$ (bound by 26.8 cm^{-1}) and $v = 45$ (bound by 4.5 cm^{-1}), respectively, and our estimates of the energies and rotational constants of all unobserved levels of both states are included in the Supplementary Data associated with this paper.[32]

Table III compares our present estimate of the potential energy well depth of ground-state NaH with selected previous values. It is noteworthy that our value differs from that of Huang *et al.* by far more than the sum of their uncertainties, although they were based on very similar data sets. We believe that this improvement illustrates the strength of our DPF procedure. As illustrated by the upper panel of figure 2, our final estimate of the uncertainty in $\mathfrak{D}_e$ is almost an order of magnitude larger than the uncertainty yielded by the final fit to our particular recommended model. This is a common effect of taking model-dependence into account. However, this averaging over models responsible for less than half of our estimated uncertainties in the physically significant A-state parameters T_e, r_e and u_0.

A widely noted fact about the $A\,^1\Sigma^+$ states of all alkali hydrides is that their vibrational spacings and B_v values initially *in*crease with v, a property that reflects the broader-than-quadratic shape of their potential minima, which in turn is associated with the influence of the transient ion-pair character of their attractive outer walls (see Fig. 1) and the associated (distant) avoided crossing with the ground state. However, Figs. 5 and 6 illustrate another interesting property, which is that over much of its well, the vibrational spacings of the $A\,^1\Sigma^+$ state of NaH are approximately constant, even though Fig. 5 shows that its shape is strongly anharmonic. This provides an unusual physical illustration of the separate roles of vibrational and rotational data in determining a potential energy function that are so clearly delineated by the two equations of the semiclassical RKR inversion procedure:[11] the vibrational spacings only depend on, and hence determine, how the width of the potential well increases with energy, and not its overall shape, so that over a substantial energy range a pure harmonic oscillator and a strongly *an*harmonic potential energy function can have

approximately the same vibrational spectrum.

Acknowledgements

We are very grateful to Professor Klaas Bergmann and Dr. Frank Pesl for providing us with the accumulated data file used in their 2000 analysis, and to Professor Y.-H. Huang for helpful communications regarding aspects of his published data set. We are also very grateful to the late Professor Jim Mitroy of Charles Darwin University (Australia) for providing us with his unpublished values of the dispersion coefficients between an H atom and an excited Na($2P$) atom, and for many other helpful communications over the years. His untimely death was a significant loss for science. This research was supported by the Natural Sciences and Engineering Research Council of Canada through a 'Discovery Grant' held by RJL.

[1] F. Crawford and J. T. Jorgenson, Phys. Rev. **47**, 358 (1935).

[2] R. Mulliken, Phys. Rev. **50**, 1017 (1936).

[3] W. C. Stwalley and W. Zemke, J. Phys. Chem. Ref. Data **20**, 153 (1991).

[4] J. Coxon and C. Dickinson, J. Chem. Phys. **121**, 9378 (2004).

[5] J. Tennyson and S. Yurchenko, Mon. Not. R. Astron. Soc. **425**, 21 (2012).

[6] J. Tennyson, in *68th International Symposium on Molecular Spectroscopy at the Ohio State University* (Columbus, Ohio, 2013), Paper TB05.

[7] T. Hori, Z. Physik **62**, 352 (1930).

[8] T. Hori, Z. Physik **71**, 478 (1931).

[9] M. Aymar, J. Deiglmayr, and O. Dulieu, Can. J. Phys. **87**, 543 (2009).

[10] G. Herzberg, *Spectra of Diatomic Molecules* (Van Nostrand, New York, 1950).

[11] (a) R. Rydberg, Z. Physik **73**, 376 (1931); (b) O. Klein, Z. Physik **76**, 226 (1932); (c) R. Rydberg, Z. Physik **80**, 514 (1933); (d) A.L.G. Rees, Proc. Phys. Soc. **59**, 998 (1947).

[12] R. J. Le Roy, `RKR1 2.0`: *A Computer Program Implementing the First-Order RKR Method for Determining Diatomic Molecule Potential Energy Curves*, University of Waterloo Chemical Physics Research Report CP-657 (2003); see `http://leroy.uwaterloo.ca/programs/`.

[13] R.J. Le Roy, *Determining Equilibrium Structures and Potential Energy Functions for Diatomic Molecules*, Chapter 6, pp. 159-203, of *Equilibrium Structures of Molecules*, J. Demaison and A. G. Csaszar editors, Taylor & Francis, London (2011).

[14] R. J. Le Roy, J. Seto, and Y. Huang, `DPotFit 2.0`: *A Computer Program for fitting Diatomic Molecule Spectra to Potential Energy Functions*, University of Waterloo Chemical Physics Research Report CP-667 (2013); see `http://leroy.uwaterloo.ca/programs/`.

[15] R. Henderson, A. Shayesteh, J. Tao, C. Haugen, P. Bernath, and R. Le Roy, J. Phys. Chem. A **117**, 13373 (2013).

[16] J. Mitroy and M. W. J. Bromley, Phys. Rev. A **68**, 062710 (2003); Erratum *ibid* **A71**, 019903(E) (2005).

[17] E. Olsson, Z. Physik **93**, 206 (1934).

[18] F. P. Pesl, S. Lutz, and K. Bergmann, Eur. Phys. J. D **10**, 247 (2000).

[19] R. Pankhurst, Proc. Phys. Soc. (London) **A 62**, 191 (1949).

[20] K. Sastry, E. Herbst, and F. D. Lucia, J. Chem. Phys. **75**, 4753 (1981).

[21] K. R. Leopold, L. R. Zink, K. M. Evenson, and D. A. Jennings, J. Mol. Spectrosc. **122**, 150 (1987).

[22] U. Magg and H. Jones, Chem. Phys. Lett. **146**, 415 (1988).

[23] A. G. Maki and W. B. Olson, J. Chem. Phys. **90**, 6887 (1989).

[24] M. Rafi, N. Ali, K. Ahmad, I. A. Khan, M. A. Baig, and Z. Iqbal, J. Phys. B: At. Mol. Opt. Phys. **26**, L129 (1993).

[25] M. Rafi, private communication (2013).

[26] S. Lochbrunner, M. Motzkus, G. Pichler, K. L. Kompa, and P. Hering, Z. Phys. D – Atoms, Molecules and Clusters **38**, 35 (1996).

[27] J. Pesl, (2012); we are grateful to Dr. Pesl for providing us with these unpublished data of Lochbrunner *et al.*[26]

[28] J. T. Bahns, C. Tsai, B. Ji, J. Kim, G. Zhao, W. Stwalley, J. Bloch, and R. Field, J. Mol. Spectrosc. **186**, 222 (1997).

[29] H.-Y. Huang, T.-L. Lu, T.-J. Whang, Y.-Y. Chang, and C.-C. Tsai, J. Chem. Phys. **133**, 044301 (2010).

[30] J. L. Dunham, Phys. Rev. **41**, 713-720 (1932); *ibid* **41**, 721-731 (1932).

[31] Our initial analyses found that in Huang *et al.*'s original data set,[29] the transition energies for the (10,16) band appeared to be systematically displaced by approximately $10\,\mathrm{cm}^{-1}$. Dr. Huang has kindly provided us with the correct values for these data (T.-J. Huang, private communication (2012)), and they were used in the present analysis.

[32] See AIP Document No. E-PAPS for ASCII files containing listings of the data used in the present work and [calc.-obs] values from our final fit, for tabulations of the vibrational energies and rotational constants all bound levels of the $X\,^1\Sigma^+$ and $X\,^1\Sigma^+$ States of NaH and NaD that were generated from our final recommended potential energy functions, for sample data files for use in performing bond-state/Franck-Condon calculations using Program LEVEL,[45] and for a FORTRAN subroutines for generating those recommended MLR and DELR potential energy functions. These files can be reached through a direct link in the online article's HTML reference section or via the EPAPS homepage (http://www.aip.org/pubservs/epaps.html).

[33] J. Watson, J. Mol. Spectrosc. **80**, 411 (1980).

[34] J. K. G. Watson, J. Mol. Spectrosc. **223**, 39 (2004).

[35] R. J. Le Roy, J. Mol. Spectrosc. **194**, 189 (1999).

[36] N. Dattani and R. Le Roy, J. Mol. Spectrosc. **268**, 199 (2011).

[37] R. J. Le Roy, `betaFIT 2.1`: *A Computer Program to Fit Potential Function Points to Selected Analytic Functions*, University of Waterloo Chemical Physics Research Report CP-666 (2013); see `http://leroy.uwaterloo.ca/programs/`.

[38] W. Stwalley, W. Zemke, and S. Yang, J. Phys. Chem. Ref. Data **20**, 153 (1991).

[39] R. Le Roy, C. Haugen, J. Tao, and H. Li, Mol. Phys. **109**, 435 (2011).

[40] H. Kreek and W. J. Meath, J. Chem. Phys. **50**, 2289 (1969).

[41] C. Douketis, G. Scoles, S. Marchetti, M. Zen, and A. J. Thakkar, J. Chem. Phys. **76**, 3057 (1982).

[42] R. J. Le Roy and Y. Huang, J. Mol. Struct. (Theochem) **591**, 175 (2002).

[43] R. J. Le Roy, J. Chem. Phys. **101**, 10217 (1994).

[44] http://physics.nist.gov/PhysRefData/ASD/levels_form.html.

[45] R. J. Le Roy, LEVEL 8.2: *A Computer Program for Solving the Radial Schrödinger Equation for Bound and Quasibound Levels*, University of Waterloo Chemical Physics Research Report CP-663 (2014); see `http://leroy.uwaterloo.ca/programs/`.

[46] R. J. Le Roy, J. Mol. Spectrosc. **191**, 223 (1998).

[47] F. Orth, W. Stwalley, S. Yang, and Y. Hseih, J. Mol. Spectrosc. **79**, 314 (1980).

[48] O. Nedelec and M. Giroud, J. Chem. Phys. **79**, 2121 (1983).

[49] M. Giroud and O. Nedelec, J. Chem. Phys. **73**, 4151 (1980).

Table I Experimental data used in the final analyses of the present work.

Isotop.	**Type**	**Unc.**$(\mathbf{cm^{-1}})$	$v(\mathbf{A^1\Sigma^+})$	$\mathbf{v(X^1\Sigma^+)}$	J range	**#Data**	**source**
NaH	electronic	$0.3-0.9$	$3-20$	$0-3$	$0-37$	1905	Hori(1930/31)[7,8]
	electronic	0.3	$4-13$	$0-1$	$0-24$	524	Olsson(1935)[17]
	electronic	1.0	$1-7$	$3-8$	0	27	Pankhurst(1949)[19]
	pure rotational	0.1	—	$3-8$	$0-32$	149	Pankhurst(1949)[19]
	pure rotational	0.1	$1-7$	—	$0-32$	186	Pankhurst(1949)[19]
	electronic	0.1	$0-1$	$6-8$	$0-33$	261	Orth(1980)[47]
	pure rotational	0.000 007	—	$0-3$	$0-1$	4	Sastry(1981)[20]
	pure rotational	0.000 003-0.000 015	—	$0-3$	$0-8$	27	Leopold(1987)[21]
	vib-rotational	$0.001-0.009$	—	$0-2$	$0-15$	26	Magg(1988)[22]
	vib-rotational	$0.001-0.002$	—	$0-3$	$0-21$	58	Maki(1989)[23]
	electronic	1.0	$12-20$	$0-1$	0	17	Rafi(1993)[24]
	synthetic MW	0.2	$13-25$	$0-1$	$0-6$	144	Rafi(1993)[24]
	electronic	$0.3-0.6$	$8-15$	0	$0-25$	298	Lochbrunner(1996)[26]
	electronic	$0.3-0.4$	$2-9$	$1-3$	0	9	Lochbrunner(1996)[26]
	electronic	0.006 & 0.31	$3-9$	$0-1$	$0-22$	126	Bahn(1987)[28]
	electronic	$0.001-0.017$	$2-8$	$6-9$	$1-29$	275	Pesl(2000)[18]
	electronic 'pump'	3.0	$7-12$	0 & 9	$0-14$	50	Huang(2010)[29]
	electronic 'probe'	2.0	$7-12$	$10-21$	$1-14$	277	Huang(2010)[29]
	vib-rotational	1.0	—	0, $9-21$	$1-14$	286	Huang(2010)[29]
					Total:	4642	
NaD	electronic	$0.05-0.15$	$7-17$	$0-1$	$0-29$	591	Olsson(1935)[17]
	pure rotational	0.000 007	—	$0-3$	$1-3$	5	Sastry(1981)[20]
	electronic	$0.30-0.50$	$4-17$	$0-4$	0	25	Lochbrunner(1996)[26]
					Total:	621	
				Total Overall:		5263	

Table II: Parameters defining the recommended MLR potential energy function for the $X\,^1\Sigma^+$ state of NaH, the EMO function for the $A\,^1\Sigma^+$ state, and the associated BOB functions, as determined from the present DPF analysis. The analysis also relied on the $X\,^1\Sigma^+$−state dispersion coefficients of Mitroy and Bromley:[16] $C_6 = 3.57502 \times 10^5$, $C_8 = 5.41796 \times 10^6$ and $C_{10} = 1.12920 \times 10^8$, all in units [$\mathrm{cm}^{-1}\,\mathrm{\AA}^m$], the damping function scaling parameter $\rho_{\rm AB} = 0.69$, and the value of the Na($3s\,^2S \rightarrow 3p\,^2P_{1/2}$) excitation energy (taken from the NIST www site[44]) that defines VLIM($A\,^1\Sigma^+$). Units of energy and length are cm^{-1} and Å.

	$X\,^1\Sigma^+$	$A\,^1\Sigma^+$
VLIM	0.0	16956.17025
T_e	0.0	22712.57025 (12200)
$\mathfrak{D}_e$	15797.4 (43)	10040.0 (43)
r_e	1.887023 (15)	3.1927 (5)
$\{p,q\}/\{q\}$	$\{6,4\}$	$\{4\}$
$r_{\rm ref}$	[3.0]	[3.0]
β_0	0.06582161	0.3620684
β_1	−4.1671619	0.131948
β_2	−5.775325	0.155548
β_3	−6.25871	0.08981
β_4	−6.34291	0.41019
β_5	−6.2056	−0.2531
β_6	−5.0814	−2.8482
β_7	−2.205	−0.0395
β_8	−1.678	13.606
β_9	−8.36	2.618
β_{10}	−14.93	−39.17
β_{11}	−11.18	−8.34
β_{12}	−3.1	66.76
β_{13}	—	10.8
β_{14}	—	−61.7
β_{15}	—	−5.
β_{16}	—	24.
$\{p_{\rm ad}, q_{\rm ad}\}/\{q\}$	$\{6,4\}$	$\{3,3\}$
u_0	0.0	−2.26 (124)
u_1	17.36	−8.
u_2	28.2	21.4
u_3	69.2	70.
u_4	−220.	—
u_∞	[0.0]	[0.0]
$\{p_{\rm na},\, q_{\rm na}\}$	$\{3,\, 3\}$	$\{3,\, 3\}$
t_0	[0.0]	[0.0]
t_1	0.00005	0.00016
t_2	−0.003	—
t_∞	[0.0]	[0.0]

Table III. Comparison of present NaH($X\,^1\Sigma^+$) well depth with some previous values.

Reference	$\mathfrak{D}_e/\mathrm{cm}^{-1}$	Method
present work (2013)	$\mathbf{15\,797.4 \pm 4.3}$	direct fit of data to analytic potential functions
Huang *et al.* (2010)[29]	$15\,815 \pm 5$	polynomial Birge-Sponer extrapolation from $v'' = 21$
Stwalley *et al.* (1991)[38]	$15\,900 \pm 100$	add *ab initio* tail to vibrational energy at $v'' = 19$
Nedelec and Grioud (1983)[48]	$15\,785 \pm 20$	polynomial Birge-Sponer extrapolation from $v = 19$
Grioud and Nedelec (1980)[49]	$16\,300 \pm 500$	polynomial Birge-Sponer extrapolation from $v = 16$
Pankhurst (1949)[19]	17 410	linear Birge-Sponer extrapolation from $v'' = 8$
Hori (1931)[8]	18 100	polynomial Birge-Sponer extrapolation from $v'' = 20$

Figure Legends

Figure 1. Potential energy functions of the lowest six $^1\Sigma^+$ states of NaH as calculated by Aymar, Deiglmayr and Dulieu:[9] solid red curves are states dissociating to neutral fragments, while the dash-dot-dot curve is the lowest state dissociating to the ion-pair limit (blue long-dash line) and the blue dotted curve shows the inward extrapolation of its limiting long-range behaviour.

Figure 2. Lower Panel: Dependence of $\overline{dd}$ on the exponent polynomial order $N = N_\beta$ and the expansion centre location $r_{\rm ref}$ for various choices of the expansion function parameters p and q, in single-state fits to data for the $X\,^1\Sigma^+$ state.

Upper Panel: fitted values of $\mathfrak{D}_e$ and their associated 95% confidence limit uncertainties for most of the cases considered in the Lower Panel.

Figure 3. Test of the long-range extrapolation behaviour of selected optimized model potential energy functions for the $X\,^1\Sigma^+$ state of NaH. In the symbols $N_{p,q}^{r_{\rm ref}}$, $N = N_\beta$ indicates the exponent polynomial expansion order, $r_{\rm ref}$ is the expansion centre location, while p and q are the integers defining the radial variables of Eqs. (8)–(10).

Figure 4. Dependence of $\overline{dd}$ on the exponent polynomial order $N = N_\beta$ and the expansion centre location $r_{\rm ref}$ for two choices of the expansion function parameter q for the $A\,^1\Sigma^+$ state in two-state fits with the $X\,^1\Sigma^+-$state model fixed, but its parameters free.

Figure 5. Lower Panel: Comparison of the *ab initio* potentials of Aymar *et al.* (round points) with the present empirical potentials (solid red and blue curves). The horizontal line segments indicate the energies of the observed vibrational levels used in the analysis, while the diagram inserts provide additional detail near the potential minima. **Upper Panel:** predicted uncertainties in the fitted potentials due to the uncertainties in the parameters determined by the fit.

Figure 6. Birge-Sponer plots for the observed vibrational levels of NaH($X\,^1\Sigma^+$) (red square points) and of NaH($X\,^1\Sigma^+$) (blue triangular points), and predicted values for the unobserved higher levels of the latter (open round points).

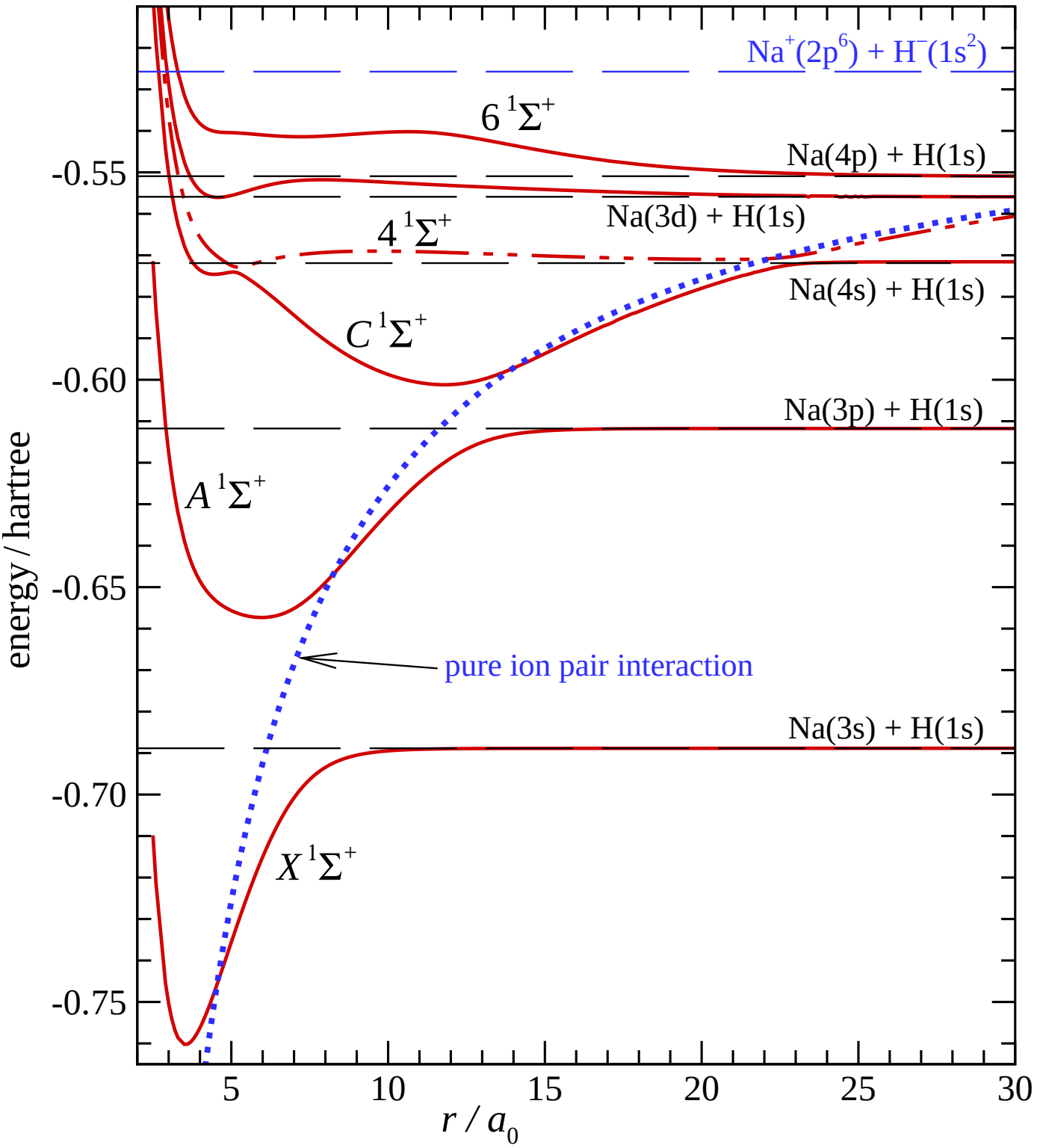

Figure 1. Potential energy functions of the lowest six $^1\Sigma^+$ states of NaH as calculated by Aymar, Deiglmayr and Dulieu:[9] solid red curves are states dissociating to neutral fragments, while the dash-dot-dot curve is the lowest state dissociating to the ion-pair limit (blue long-dash line) and the blue dotted curve shows the inward extrapolation of its limiting long-range behaviour.

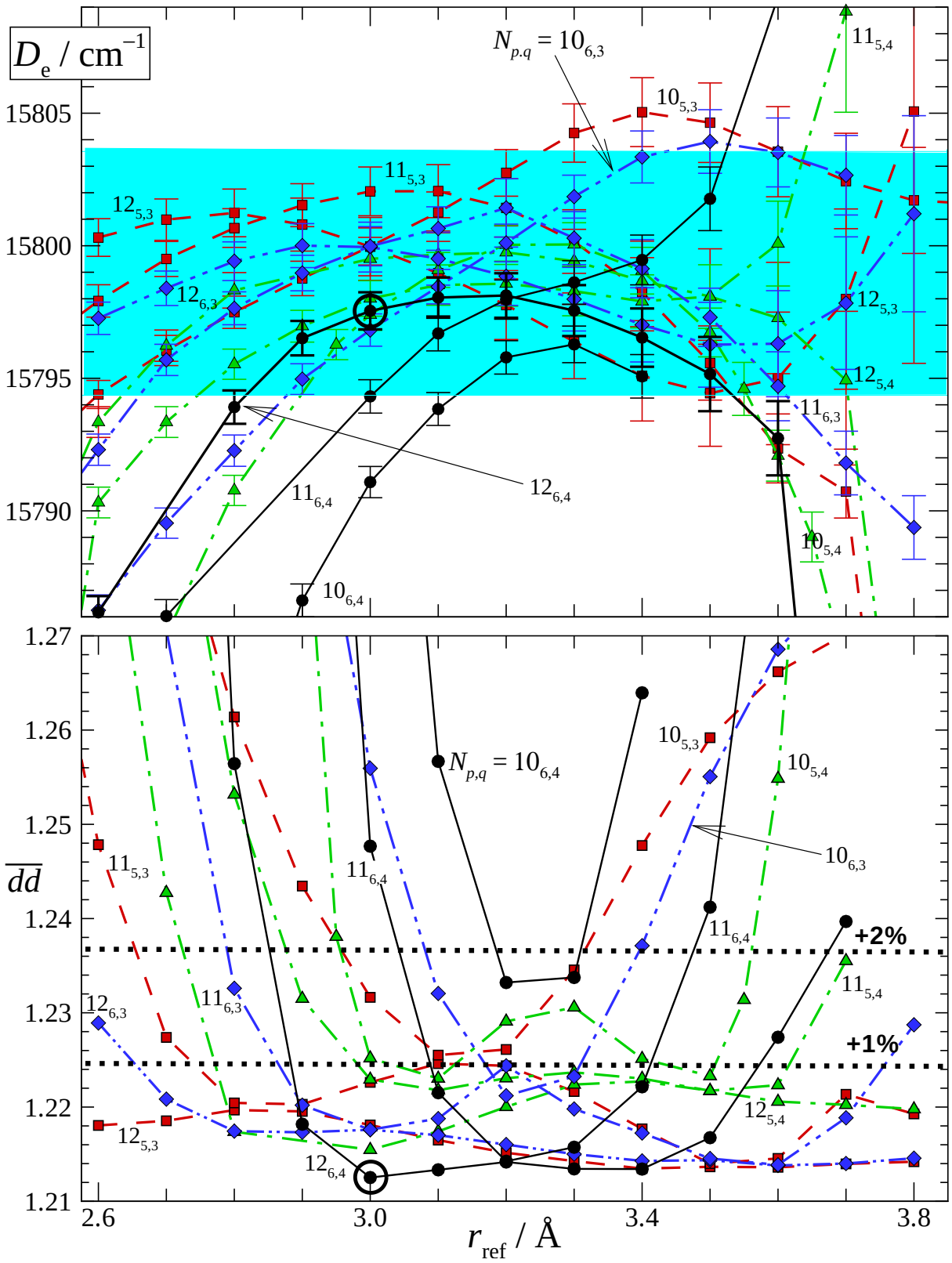

Figure 2. Lower Panel: Dependence of $\overline{dd}$ on the exponent polynomial order $N = N_\beta$ and the expansion centre location $r_{\rm ref}$ for various choices of the expansion function parameters p and q, in single-state fits to data for the $X\,^1\Sigma^+$ state.

Upper Panel: fitted values of $\mathfrak{D}_e$ and their associated 95% confidence limit uncertainties for most of the cases considered in the Lower Panel.

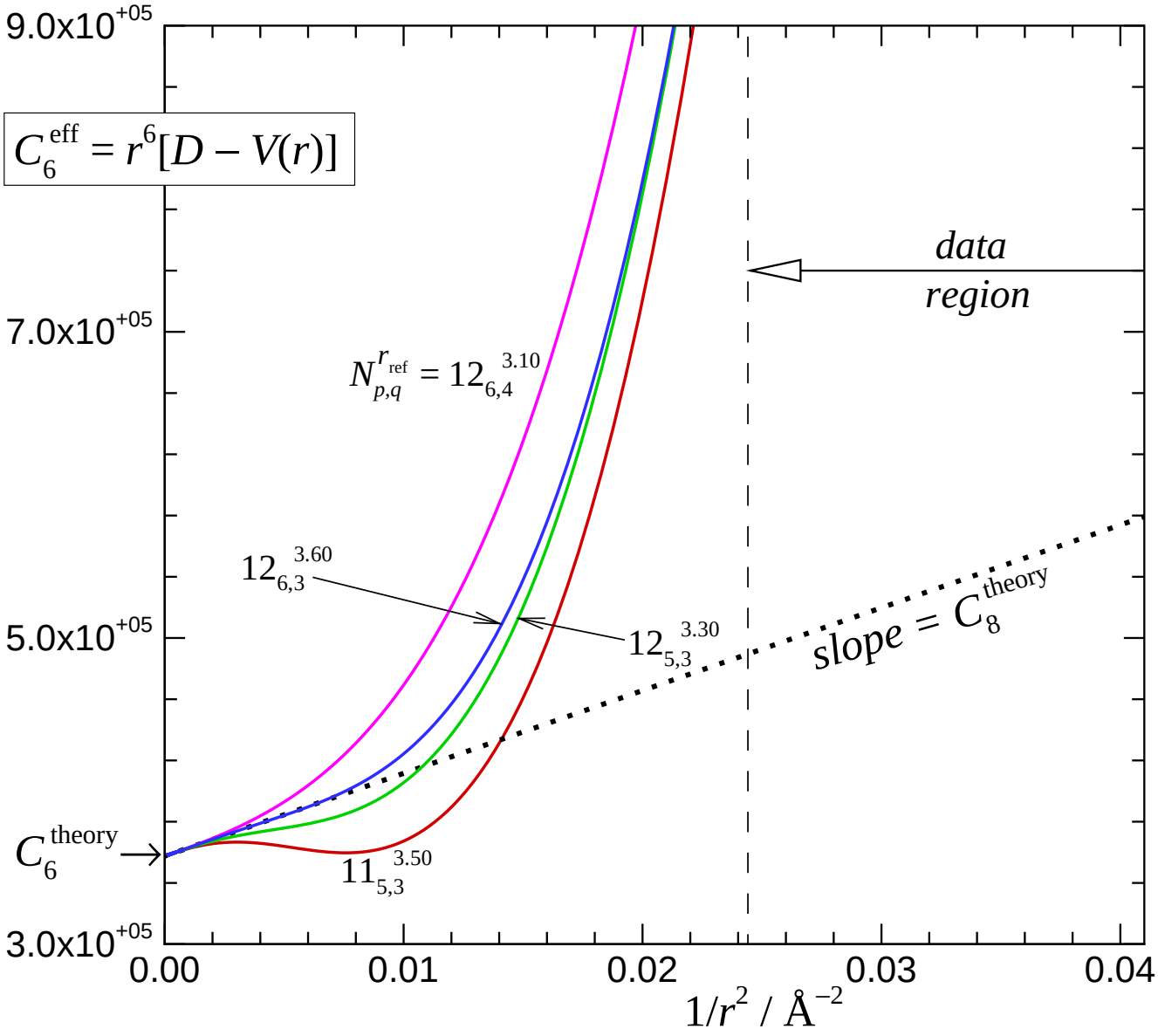

Figure 3. Test of the long-range extrapolation behaviour of selected optimized model potential energy functions for the $X\,^1\Sigma^+$ state of NaH. In the symbols $N_{p,q}^{r_{\text{ref}}}$, $N = N_\beta$ indicates the exponent polynomial expansion order, r_{ref} is the expansion centre location, while p and q are the integers defining the radial variables of Eqs. (8)–(10).

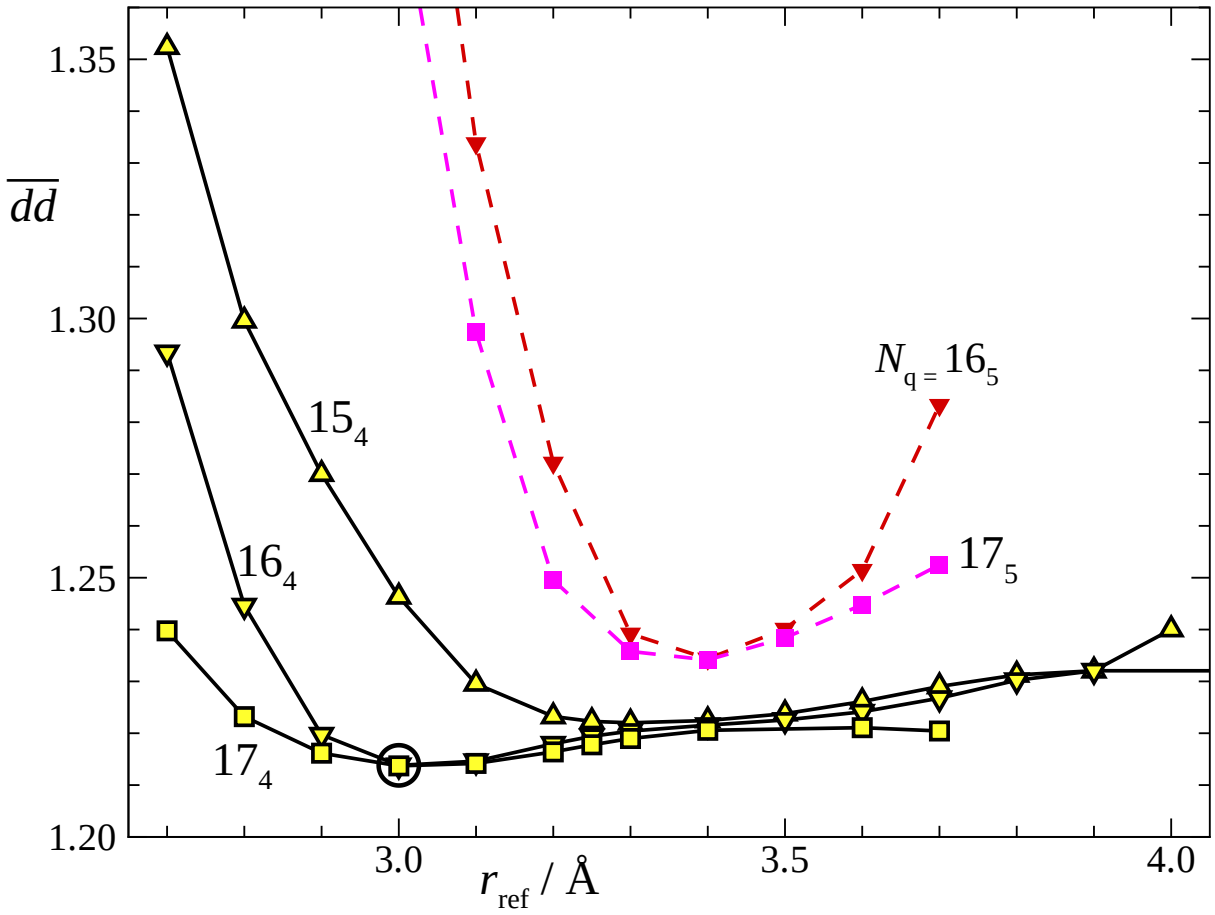

Figure 4. Dependence of $\overline{dd}$ on the exponent polynomial order $N = N_\beta$ and the expansion centre location r_{ref} for two choices of the expansion function parameter q for the $A\,^1\Sigma^+$ state in two-state fits with the $X\,^1\Sigma^+-$state model fixed, but its parameters free.

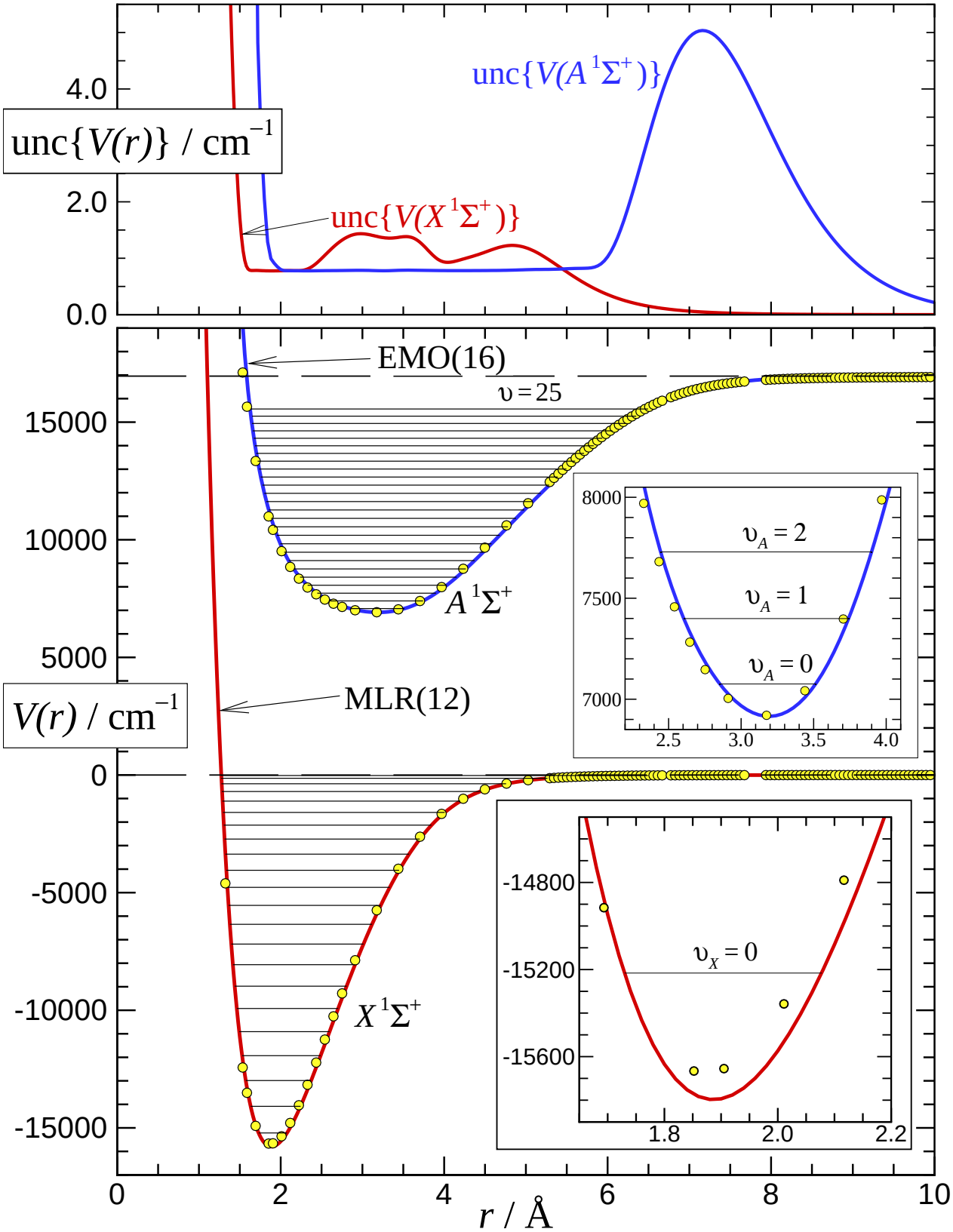

Figure 5. Lower Panel: Comparison of the *ab initio* potentials of Aymar *et al.* (round points) with the present empirical potentials (solid red and blue curves). The horizontal line segments indicate the energies of the observed vibrational levels used in the analysis, while the diagram inserts provide additional detail near the potential minima. **Upper Panel:** predicted uncertainties in the fitted potentials due to the uncertainties in the parameters determined by the fit.

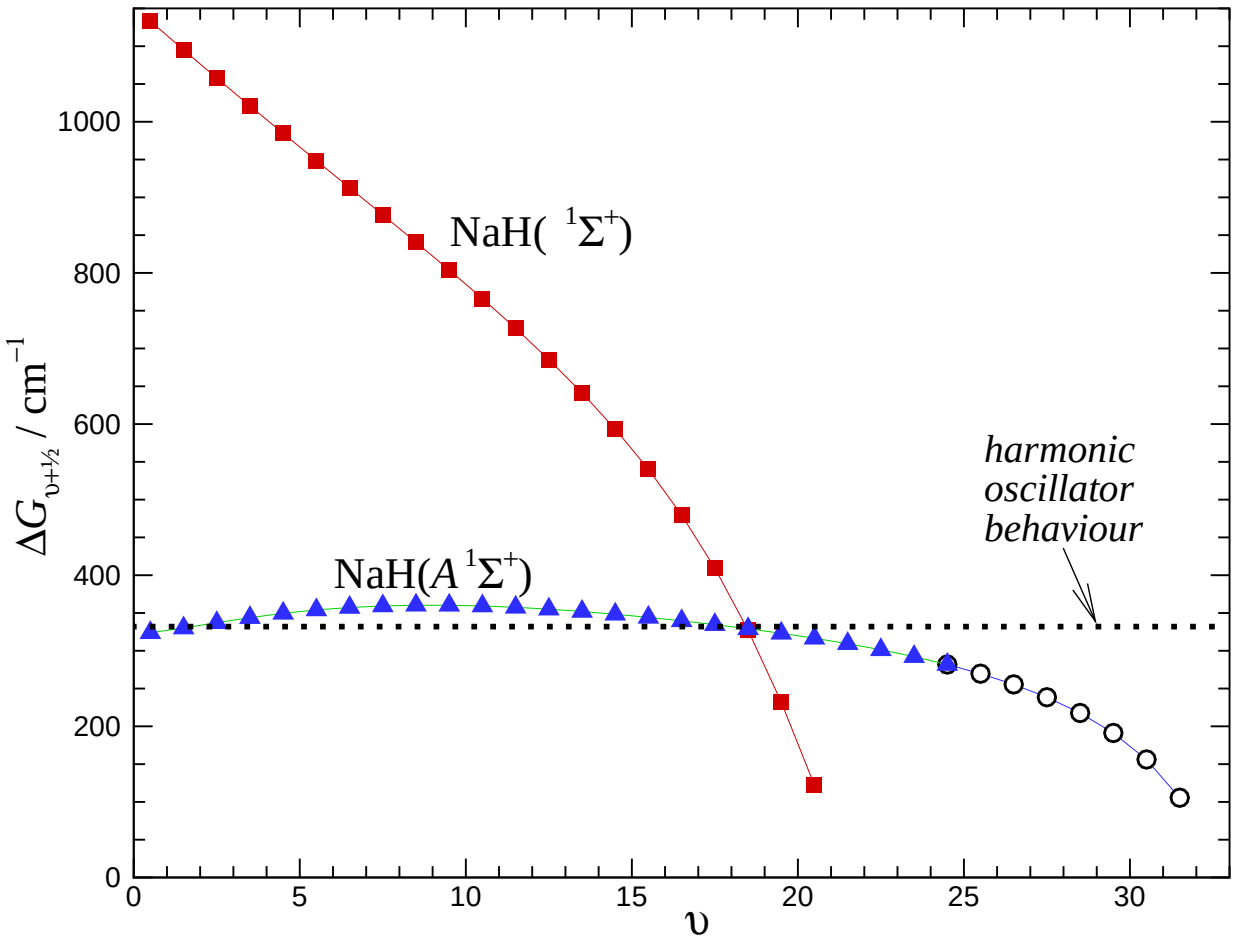

Figure 6. Birge-Sponer plots for the observed vibrational levels of NaH($X\,^1\Sigma^+$) (red square points) and of NaH($X\,^1\Sigma^+$) (blue triangular points), and predicted values for the unobserved higher levels of the latter (open round points).